Towards new zero-thermal-expansion materials: Li-free quartz solid solutions stuffed with transition metal cations

Haytem Bazzaoui, Cecile Genevois, Emmanuel Véron, Michael J Pitcher, Mathieu Allix, Alessio Zandonà

Towards new zero-thermal-expansion materials: Li-free quartz solid solutions stuffed with transition metal cations

Haytem Bazzaoui[1], Cécile Genevois[1], Emmanuel Véron[1], Michael J. Pitcher[1], Mathieu Allix[1], Alessio Zandonà[1,*]

[1] CNRS, CEMHTI UPR3079, Univ. Orléans, F-45071 Orléans, France

Abstract

Stuffed aluminosilicate quartz solid solutions (Qss) represent the main functional component of state-of-the-art zero-thermal-expansion glass-ceramics. For the first time, we present the synthesis of Li-, Mg- and Zn-free Qss solely stuffed with transition metal cations (Fe^{2+}, Ni^{2+}, Co^{2+}); partial Li^{+} co-doping enables also significant Mn^{2+} incorporation. They were obtained by glass powder crystallization; Qss crystals exhibit compositionally tunable coefficients of thermal expansion (CTEs), from $-2x10^{-6}$ K^{-1} to $\sim 10x10^{-6}$ K^{-1} in the range 30–300 °C. Co^{2+}-bearing crystals exhibit the closest-to-zero CTE value ($0.2x10^{-6}$ K^{-1}) and the most isotropic behavior in the whole Qss family, opening up new perspectives for the development of Li-free low-expansion materials. From a structural point of view, we identified the unit cell volume (and not the pseudo-hexagonality of the aluminosilicate framework) as the key structural parameter leading to low or negative CTEs in Qss, with a linear correlation extending to non-stuffed non-silicate quartz-like phases.

Keywords: stuffed quartz solid solutions; zero thermal expansion; aerodynamic levitation; transition metal cations; glass crystallization.

***Corresponding author:** alessio.zandona@cnrs-orleans.fr

1.Introduction

Low quartz (or α-quartz, SiO_2) represents the most common crystalline component of Earth's continental crust. Its structure (enantiomorphic space groups: $P3_121$ or $P3_221$) consists of interconnected helical chains of SiO_4 tetrahedra (Fig. S1 of the Supplementary Materials), defining continuous trigonal channels running along the *c*-axis [1]. This framework transforms reversibly upon heating above 573 °C, assuming hexagonal symmetry (high or β-quartz, enantiomorphic space groups: $P6_422$ or $P6_222$). Notably, the same temperature marks a striking transition from positive to almost null thermal expansion, as reported by Le Châtelier at the end of the XIX century [2].

Although its piezoelectric properties have been essential for metrology and telecommunications since the 1930s [3], the technological interest of quartz boomed by the 1960s, due to: (i) the discovery of the negative thermal expansion behavior [4] of β-eucryptite ($LiAlSiO_4$); (ii) the identification of this phase as a stuffed derivative [5] of the high quartz structure [6], in which Al^{3+} isomorphously substitutes Si^{4+}, enabling the incorporation of Li^+ at otherwise vacant channel sites; (iii) the serendipitous invention of glass-ceramics [7], in which stuffed quartz solid solutions [8,9] (Qss) with generalized formula $M_xAl_xSi_{1-x}O_2$ (M = Li, $Mg_{0.5}$ and $Zn_{0.5}$) are easily synthesized by controlled glass crystallization [10]. This combination rapidly led to the development of zero-thermal-expansion glass-ceramic materials, which are still today essential for applications spanning from transparent fire-viewing windows to telescope mirror substrates [11,12]. Between 0 °C and 50 °C, commercially available materials based on Qss such as Zerodur® can achieve a coefficient of thermal expansion (CTE) as low as $(0 \pm 0.007) \times 10^{-6}\ K^{-1}$, with spatial variations that are less than $0.005 \times 10^{-6}\ K^{-1}$ over the whole volume of a telescope mirror blank with a diameter of 4 meters [13,14]. Indeed, the thermal expansion of Qss can be finely tuned, taking advantage of their variable Al/Si ratio and of the full solid solution [8,9,15,16] existing between: (i) Mg-bearing Qss, exhibiting trigonal symmetry and positive thermal expansion [17–21]; (ii) Li- and Zn-bearing Qss, which were reported to be fully hexagonal (at a sufficiently high level of chemical stuffing) and to contract upon heating [8,12,22–27].

Qss additionally allow for a wide range of substitutions at their tetrahedral framework sites, also in absence of channel stuffing: quartz-like BeF_2, PON, GeO_2, BPO_4, $AlPO_4$, $FePO_4$, $GaPO_4$, $BAsO_4$, $AlAsO_4$ and $GaAsO_4$ (referred to as "non-stuffed" in the following) were described in the past [28–34], although only P^{5+} incorporation has found application in glass-ceramics [9,11,12,35]. Moreover, the available literature hints at an even wider range of compositional variability for Qss than systematically investigated so far. Although precise structural characterization is lacking, previous authors inferred the fortuitous formation of SiO_2-rich Qss stuffed to a limited extent with Fe^{2+} and Cu^{2+} ions during the reaction between metal oxides and kaolinite [17,36–38]; concurrently, minor accommodation (at doping levels) of Mn^{2+}, Co^{2+} and Ni^{2+} has been inferred spectroscopically in lithium aluminosilicate Qss crystals formed in glass-ceramics [9,39,40]. We similarly assumed partial incorporation of Ti^{4+} in the tetrahedral sites of Li-bearing Qss (Al/Si ratio equal to 1) after devitrification [41]. Finally, Qss with formulas $HAlSi_2O_6$, $Na_{0.5}H_{0.5}AlSi_2O_6$ and $Al_{0.27}Al_{0.82}Si_{2.18}O_6$ were obtained by ion exchange and leaching [25,42].

In this study, we demonstrate the first deliberate synthesis of aluminosilicate Qss solely stuffed with Co^{2+}, Ni^{2+} and Fe^{2+}; we additionally explored simultaneous stuffing with two transition metals (i.e. Co^{2+} and Ni^{2+}) and exploited Li^+ co-doping to introduce also Mn^{2+} in the Qss structure. We obtained such crystalline phases through controlled crystallization of aluminosilicate glasses containing high amounts of transition metal oxides, produced by aerodynamic levitation coupled to laser heating (ADL). The

crystallographic characterization of these phases and the elucidation of their thermal expansion behavior enabled us to develop an unprecedentedly complete description of structure-property relationships in this class of materials. As for Co-bearing Qss in particular, their CTE was found to be the closest to zero and the most isotropic in the system, opening up alternative scenarios for the sustainable production of Li-free low-expansion materials in a global economic system that features increasing pressure on lithium resources for battery production [43].

2. Experimental

2.1 Glass synthesis and crystallization

The main target stoichiometry was $MO/M_2O \cdot Al_2O_3 \cdot 2.5SiO_2$ ($M_{0.44}Al_{0.44}Si_{0.56}O_2$, with M = Li, $Mg_{0.5}$, $Zn_{0.5}$, $Co_{0.5}$, $Ni_{0.5}$, $Mn_{0.5}$ or $Fe_{0.5}$) corresponding to the mineral cordierite ($Mg_2Al_4Si_5O_{18}$) and therefore slightly SiO_2-richer than the Li-bearing endmember β-eucryptite ($Li_{0.5}Al_{0.5}Si_{0.5}O_2$). These samples are recalled as *M*Qss in the following (e.g. CoQss for the Co-bearing sample). To explore the mutual solid solution between different stuffing cations, also a sample corresponding to a 1:1 mixture of CoQss and NiQss was produced ($Co_{0.5}Ni_{0.5}$Qss). In the case of MnLiQss, a molar substitution of 25% MnO_2 by Li_2O in the starting batch was applied, since the Li-free sample invariably yielded a complex crystalline mixture, in which Qss (if present at all) only represented a minor phase. To explore the solid solution extent towards pure SiO_2, the composition $CoO \cdot Al_2O_3 \cdot 4.6\ SiO_2$ (corresponding to 70 mol% SiO_2) was also tested (sample named CoQssSi). All nominal compositions are associated to the respective label in Table 1.

Laboratory-grade precursors were used for the syntheses: SiO_2 (99.9%, Chempur), Al_2O_3 (99.999%, Strem Chemicals), Li_2CO_3 (99%, Aldrich), MgO (99.5%, Strem Chemicals), ZnO (99.999%, Strem Chemicals), Co_3O_4 (99.9985%, Alfa Aesar), NiO (99.9%, Aldrich), MnO_2 (99.9%, Alfa Aesar), FeO (99.9%, Aldrich). The raw powder materials were dispersed in ethanol, mixed thoroughly in an agate mortar and pressed into pellets of 1 g. Small chunks (20-40 mg) were then melted using the ADL system already detailed elsewhere [44], consisting of two CO_2 lasers (maximum power: 250W) heating the sample from above and below while it levitates on an Ar gas flow. The laser power was increased until full melting was achieved, kept for 5 seconds for homogenization and then cut off to quench the melt into glass beads. The maximum achieved temperatures were approximately 1800–2000 °C as from pyrometer reading; no evident signs of volatilization (e.g. visible smoke or material deposition on the nozzle walls) were detected using this procedure.

Crystallization heat treatments were applied to powders obtained after grinding together several melt-quenched beads in an agate mortar. For most of the samples, annealing was performed in air in a laboratory furnace at temperatures carefully **selected (summary in Tab. 1) by trial and error to**

maximize the amount and unit cell volume of Qss (i.e. their degree of structural stuffing) while minimizing the appearance of secondary phases, also based on previous works on Li- and Mg-bearing Qss [21,23]. FeQss proved more sensitive to the redox conditions and could therefore only be transformed into Qss when the heat treatments took place in vacuum: we particularly used an Anton Paar's HTK1200N heating chamber attached to a diffractometer to monitor the process, quickly cooling the sample after the formation of Qss to avoid its decomposition.

We also unsuccessfully explored the possibility of crystallizing Qss stuffed with other transition metal cations (Cr and Cu): in the case of chromium, the strong liquid immiscibility in the system [45] prevented the synthesis of a homogeneous aluminosilicate glass even with the addition of some Li_2O; as for copper, our synthesis conditions (even trying with an O_2 atmosphere) appeared to stabilize Cu^+ rather than Cu^{2+} and, after adjusting the stoichiometry, we were only able to obtain keatite solid solutions (another aluminosilicate stuffed derivative of SiO_2 [46,47]) as described by previous authors [48].

2.2 Powder diffraction

Laboratory X-ray powder diffraction (PXRD) measurements were performed in Bragg-Brentano geometry on a D8 Advance Bruker diffractometer (Cu Kα radiation) equipped with a LynxEye XE line detector. The samples were either dispersed on low-background flat Si holders using an ethanol mull, or compacted in front-loading Si holders, according to the available amount of powder. To estimate the amorphous fraction in sample CoQss, a weighed-in CaF_2 fully crystalline standard was used. Samples ZnQss, CoQss, NiQss and FeQss were additionally characterized by synchrotron powder diffraction (SPD) using the mail-in service of the 11BM beamline at the Advanced Photon Source at Argonne National Laboratory (USA). The powders were loaded into 0.8 mm Kapton capillaries and measured in the range 0-50° 2θ (calibrated wavelength: 0.458162 Å) with increments of 0.001° 2θ. CoQss was characterized by neutron powder diffraction (NPD) on the instrument MEREDIT at the Nuclear Physics Institute of the Czech Academy of Sciences (λ = 1.46 Å, range 4−144° 2θ, 0.08° increments, total measuring time ~27 h). For this specific measurement, approximately 4 g of powder were obtained by crushing numerous amorphous beads synthesized by ADL, subsequently crystallizing them at 850 °C for 45 min.

The thermal expansion of **Qss phases contained in the samples** was determined **by variable temperature PXRD (VT-PXRD)** using an Anton Paar HTK1200N furnace mounted on a D8 Advance Bruker laboratory diffractometer, acquiring a diffractogram every 50 °C between 30 and 600 °C. Silicon powder was added to the samples as an internal standard, to correct at each temperature for the height displacement due to the dilatation of the Al_2O_3 sample holder; pure quartz (99.9% SiO_2, Chempur) was measured in the same way for comparison. Lattice parameters were extracted from PXRD data by Le Bail

refinements, performed with the software HighScore Plus (Panalytical); full structural refinements of SPD and NPD data were carried out using TOPAS Academic (v.6) [49].

2.3 Transmission electron microscopy (TEM)

Electron energy loss spectroscopy (EELS) measurements were performed on Qss crystallites from samples CoQss, NiQss, and MnLiQss. A JEOL ARM200F cold FEG TEM operating at 80 kV was used due to the very limited stability of the samples under the electron beam. Small amounts of powder were ground and suspended in ethanol in an agate mortar; a small droplet of each suspension was then deposited onto a copper grid layered by a holey amorphous carbon film. After quick exploration in TEM mode, the samples were characterized in scanning mode (STEM). Energy-dispersive X-ray spectroscopy (EDX) was used to confirm the composition of the areas to be measured, which invariably matched the nominal one within uncertainty. Subsequently, we acquired EELS spectra (dispersion: 0.4 eV/channel) simultaneously at low (zero-loss-peak) and high (the target absorption edge) energy loss, integrating data over raster maps of several nanometers to minimize the effects of beam damage. The thickness-to-wavelength ratio during EELS spectra was kept in the range 0.4-0.6 to minimize plural scattering events. During the processing, EELS spectra were realigned according to the respective zero-loss peak and de-convoluted to correct plural scattering events using the software DigitalMicrograph GMS 3 (Gatan). They were then qualitatively compared to the spectra obtained from available laboratory-grade single-valence simple oxides measured under the same conditions, namely $LiCoO_2$, NiO, MnO and MnO_2.

3. Results

Table 1. Overview of the synthesized samples, summarizing their nominal compositions, applied heat treatments, lattice parameters and PXRD-derived CTE values obtained for Qss (space group $P3_221$) and the presence of minor secondary phases (identified from PXRD data shown in Fig. 1 and SPD data in Fig. 4). Abbreviations: *n.m.* for "not measured", *mul* for mullite, *sp* for aluminate spinel, *NiO* for nickel (II) oxide, *Ni* for metallic nickel, *mag* for magnetite, *un* for unidentified secondary phase(s), ***rg* for a substantial fraction of residual glass**.

Sample	Nominal composition	Heat treatment (°C, min)	Qss parameters		Qss CTE 30–300 °C (10^{-6} K^{-1})	Secondary phases
			a (Å)	*c* (Å)		
LiQss	$Li_{0.44}Al_{0.44}Si_{0.56}O_2$	950, 30	5.2643(2)	5.4776(3)	-0.7	-none-
MgQss	$Mg_{0.22}Al_{0.44}Si_{0.56}O_2$	950, 240	5.2087(2)	5.3459(3)	3.7	mul, sp
ZnQss	$Zn_{0.22}Al_{0.44}Si_{0.56}O_2$	950, 30	5.27690(3)	5.45340(5)	-2.2	mul, sp
CoQss	$Co_{0.22}Al_{0.44}Si_{0.56}O_2$	850, 30	5.26201(3)	5.41686(5)	0.2	mul**, rg**
CoQssSi	$Co_{0.15}Al_{0.30}Si_{0.70}O_2$	950, 30	5.193(2)	5.420(3)	n.m.	mul**, rg**
$Co_{0.5}Ni_{0.5}$Qss	$Co_{0.11}Ni_{0.11}Al_{0.44}Si_{0.56}O_2$	900, 30	5.2541(5)	5.3991(8)	1.9	Mul
NiQss	$Ni_{0.22}Al_{0.44}Si_{0.56}O_2$	900, 30	5.25207(5)	5.37512(8)	2.2	sp, NiO, Ni**, rg**
FeQss	$Fe_{0.22}Al_{0.44}Si_{0.56}O_2$	775, 15	5.23177(3)	5.37774(5)	3.0	mul, mag**, rg**
MnLiQss	$Mn_{0.16}Li_{0.12}Al_{0.44}Si_{0.56}O_2$	850, 30	5.2511(4)	5.3744(6)	2.4	un

Based on the negligible volume nucleation observed for Li-, Mg- and Zn-bearing Qss in glasses and melts devoid of nucleating agents [8,50–52], finely ground glass powders (Fig. S2) were subjected to very short heat treatments to induce instantaneous surface nucleation and growth of Qss phases, minimizing diffusion and phase separation tendency in the initially homogeneous glasses and avoiding thermal decomposition of the formed phases. As confirmed by PXRD (Fig. 1), this approach allowed Qss to be obtained as the main crystalline component in all samples listed in Table 1, despite the pronounced metastability of these phases. The applied chemical substitutions induced substantial changes in the relative intensities of their diffraction peaks, evident for example from the (010) and (110) reflections, respectively at ~19.5° and ~34° 2θ: while well-visible in LiQss and MgQss, these reflections almost completely disappeared in the samples stuffed with heavier transition metal cations. The chosen synthesis route led to a considerable amount of residual vitreous phase, as evidenced by some of the PXRD measurements shown in Figure 1: an estimation of the amorphous fraction in sample CoQss yielded 64(6) wt% using a weighed-in CaF_2 standard, for instance. The most frequent secondary phases (between 2 and 10 wt% of the crystalline fraction, depending on the sample) included mullite and aluminate spinel, as expectable from the starting compositions and from previous investigations of Mg-bearing Qss [21]. Although *a*- and/or *c*-doubling have been reported in the literature for Li- and Mg-bearing Qss and assigned to Al/Si ordering in the tetrahedra and non-random distribution of stuffing cations in the

channels [19,53], low-temperature glass crystallization was shown to yield virtually fully disordered crystals [54]. While PXRD measurements performed on LiQss and MgQss did not allow unambiguous identification of such structural features, SPD and NPD measurements (presented below) clearly excluded the occurrence of superstructure peaks in ZnQss, CoQss, NiQss and FeQss. We therefore based our further analysis uniquely on the substructure common to all Qss (space group $P3_221$), also to facilitate their comparison.

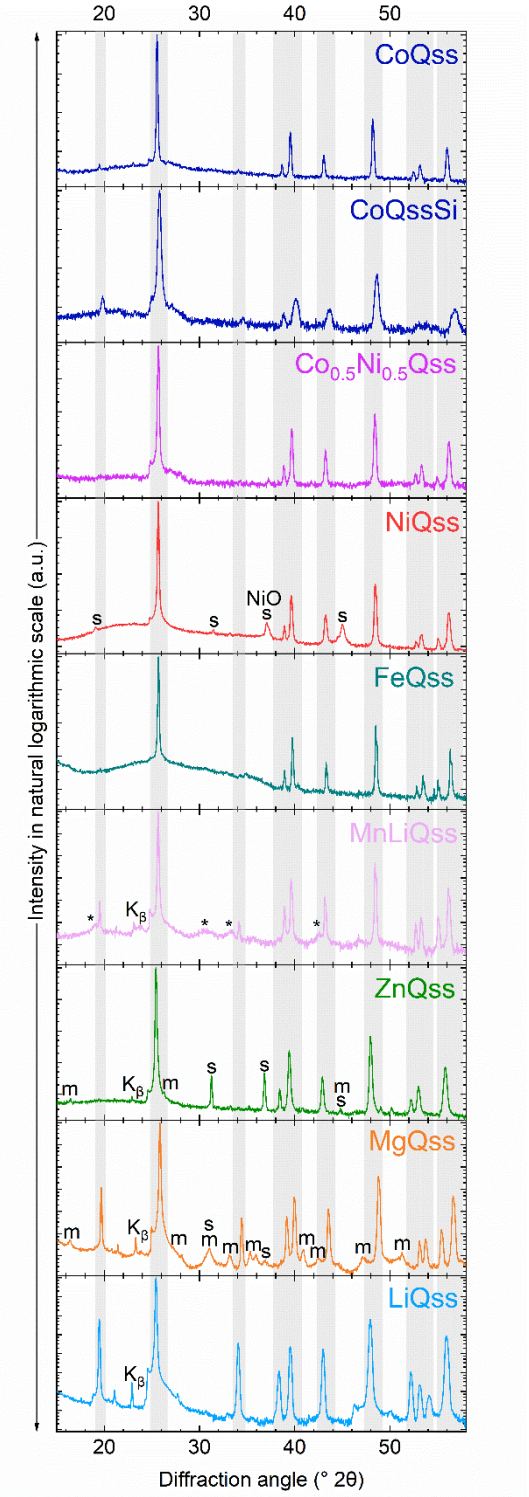

Figure 1. Excerpts of PXRD patterns (y-axis in natural logarithmic scale) collected from quartz solid solutions (Qss) synthesized within this work. Gray-shaded areas highlight peaks pertaining to Qss phases (note the systematic shifts produced by stuffing with different cations), which were the main crystalline component in all samples; otherwise labelled peaks arose from secondary phases: *m* for mullite, *s* for aluminate spinel, *NiO* for nickel (II) oxide, * for unassigned peaks. K_β marks the Cu-K_β line diffracting as the main peak of Qss.

We performed EELS measurements on Qss crystals contained in samples CoQss, NiQss and MnLiQss to investigate the oxidation state of the transition metal ions in the phases, although their instability under the electron beam and their relatively low metal contents led to spectra with poor signal-to-noise ratios compared to the standards $LiCoO_2$, NiO, MnO and MnO_2 (Fig. 2). The qualitative comparison with spectra collected from reference materials strengthened the assumption of a prevalently reduced state (Co^{2+} and Ni^{2+}) in CoQss and NiQss, corresponding to a shift of the L_3/L_2 edge of the transition metal to lower energies as compared to higher oxidation states [55–57]. As for the spectrum obtained from MnLiQss, the average manganese oxidation state was clearly higher than M^{2+}, possibly accounting for the need to co-dope the material with Li^+ to induce the formation of Qss. The oxygen K-edge spectra (Fig. S3) were dominated by the interactions with Si^{4+} and Al^{3+} in the structure: they were therefore very similar in all three samples and markedly different from that of the reference transition metal oxides.

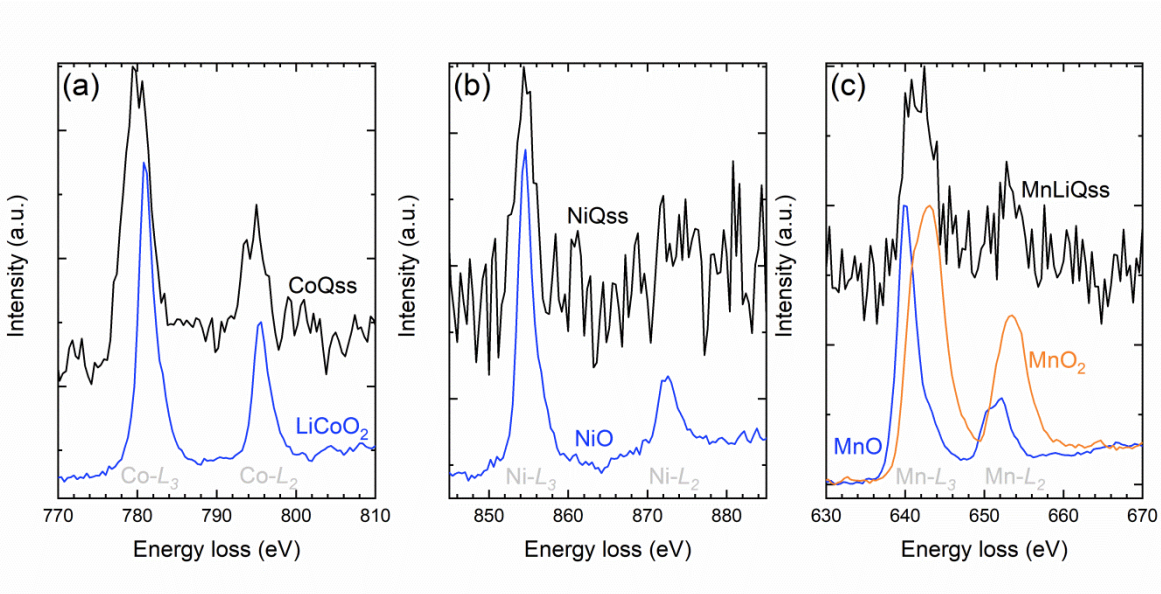

Figure 2. EELS measurements collected at the $L_{2,3}$-edge of the respective stuffing transition metal cation in samples: a) CoQss, b) NiQss, c) MnLiQss. The spectra have been renormalized and shifted vertically to facilitate the comparison with the available reference materials ($LiCoO_2$, NiO, MnO, MnO_2).

Lattice parameters (Tab. 1) were computed for all Qss, by Le Bail refinements of PXRD data or by Rietveld structural refinements for the samples measured by SPD, i.e. ZnQss, CoQss, NiQss and FeQss. Comparison of these values with the most relevant literature sources on quartz-like phases [6,16,19,21–23,25,30,33,34,42,53,58–64] confirmed the obtainment of novel stuffed derivatives of the quartz structure with distinctive structural features (Fig. 3). Indeed, our LiQss, ZnQss and MgQss plotted close to the values reported for analogous materials in the references, whereas all other Qss synthesized

within this work located at intermediate positions between ZnQss and MgQss. Mixed cation stuffing was successful in $Co_{0.5}Ni_{0.5}$Qss and yielded a unit cell with intermediate dimensions between the endmembers CoQss and NiQss. Sample CoQssSi displayed instead a noticeably shorter *a*-parameter than CoQss, in agreement with the trends observable in the Li- or Mg-bearing systems upon a change in the Al/Si ratio (and therefore in the stuffing degree) of the crystals [21,23,53].

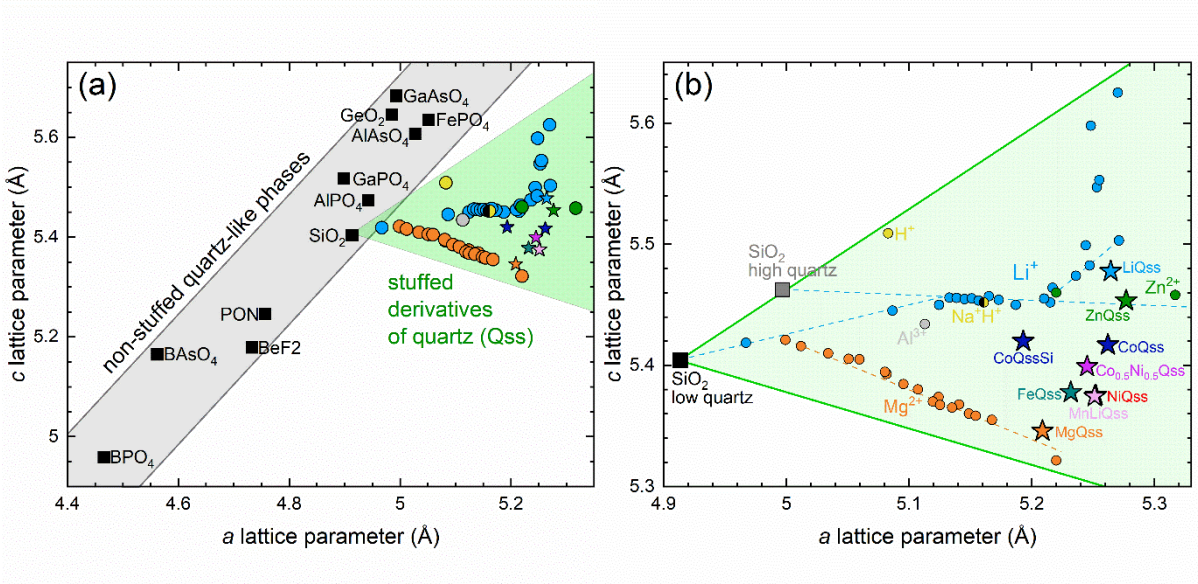

Figure 3. a) All relevant crystalline phases with a stuffed or non-stuffed quartz-like framework reported in the literature, plotted according to their *a* and *c* lattice parameters from the most reliable sources (see related text for all citations). b) Magnification of the area shaded in green, comprising all known stuffed derivatives of the quartz structure; the samples synthesized within this work are depicted as stars. Error bars are smaller than the depicted symbols.

Rietveld refinements were performed on SPD data acquired from ZnQss, CoQss, NiQss, and FeQss. Preliminary attempts using non-stuffed quartz models (i.e. trigonal or hexagonal frameworks with empty channel sites) expectedly resulted in evident peak intensity misfits; the substitution of the M^{2+} cations (M = Zn, Co, Ni, Fe) for Li^+ in the hexagonal structure of Li-bearing Qss similarly led to poor fits (Tabs. S5–S16 of the Supplementary Materials). Consequently, we adopted a refinement strategy comparing the visual quality and goodness of fit (GOF) for trigonal frameworks in which M^{2+} cations occupied: (i) solely the distorted 4-coordinated channel sites located at (0,0,0) as in Li-bearing Qss [26], labelled as T_{ch} in the following; (ii) only the distorted 6-coordinated channel sites located at (0,0,½) as in Mg-bearing Qss [19,21], labelled as O_{ch}; (iii) both T_{ch} and O_{ch} simultaneously and independently. The latter solution invariably yielded far better looking refinements (Fig. 4 and Tabs. S1–S4), showing the lowest GOF values and the best-fitting total site occupation factors (sof) as compared to the nominal composition of the samples (Fig. 5, theoretical M^{2+} sof = 0.22). Although the GOF improvement was only marginal in ZnQss and FeQss as compared to structural models comprising only one M^{2+} position

(respectively T_{ch} and O_{ch}), we refined all data using this same approach to favor the comparison across the four samples. Notice that mixed channel site occupation was also reported in the only previous structural refinement of Zn-bearing Qss [27].

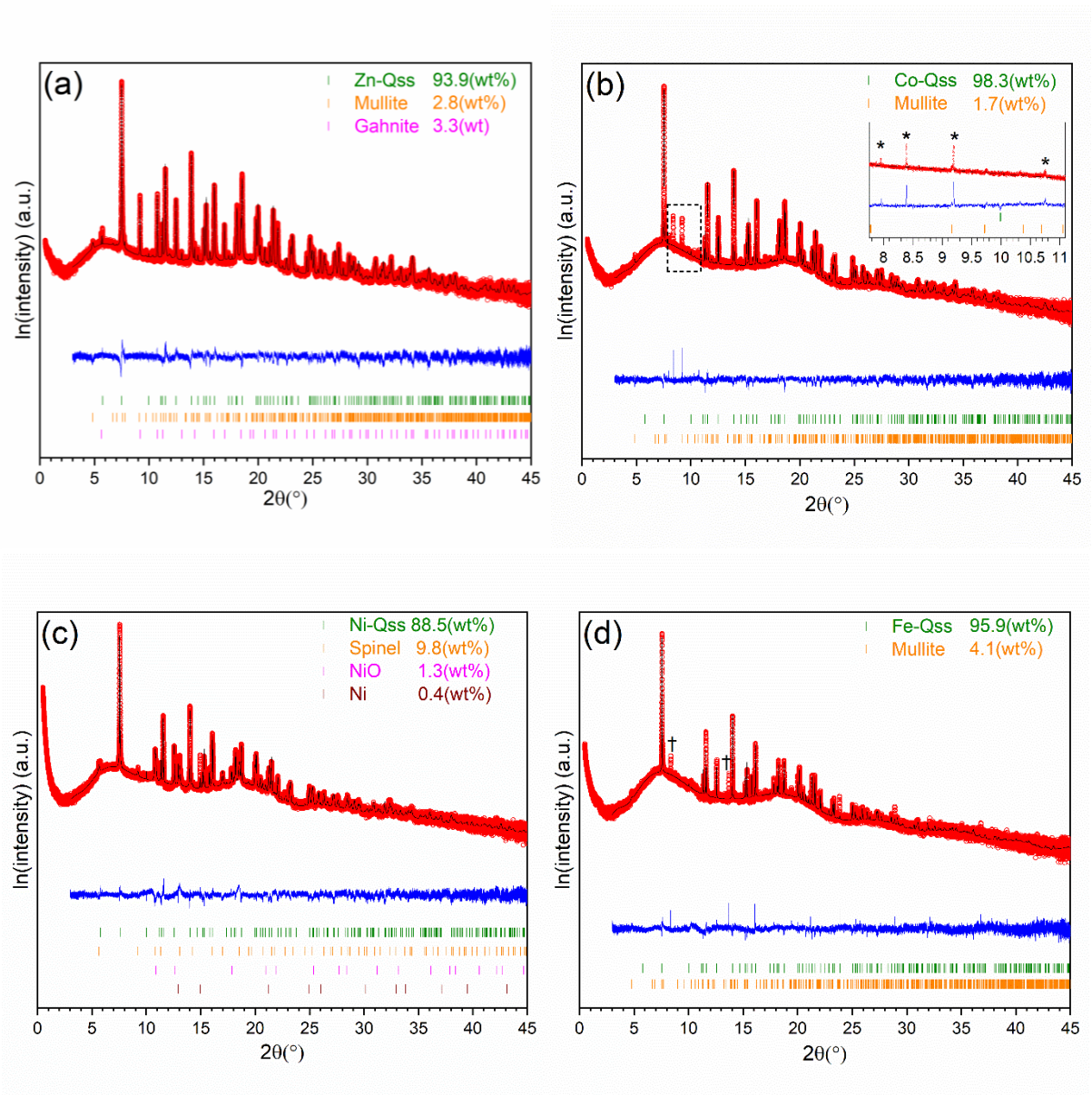

Figure 4. Rietveld refinements of SPD data (y-axis in natural logarithmic scale) collected from: a) ZnQss (R_{wp} = 9.61, GOF = 1.94), b) CoQss (R_{wp} = 6.08, GOF = 1.54), c) NiQss (R_{wp} = 7.52, GOF = 1.76) and d) FeQss (R_{wp} = 6.16%, GOF = 1.33). The shown results correspond to the best fits, obtained with structures comprising stuffing cations occupying both T_{ch} and O_{ch} positions simultaneously and independently. Measured intensities are shown in red, calculated intensities in black, residuals in blue. The peaks designated with * could not be indexed in CoQss (absent in lab PXRD and NPD); † marks the peaks of a weighed-in Si standard in FeQss.

We chose to fix all B_{iso} thermal displacement parameters to the value of 1 Å^2, which was in the range of those previously determined for all atoms by coupled SPD and NPD in a Qss of composition $LiAlSiO_4$ [54]. In fact, our B_{iso} refinement for the M^{2+} cations invariably exhibited a strong correlation with their sof (observed from the correlation matrix); we estimated a variation by as much as ~15% and ~7% of the sof determined at T_{ch} and O_{ch} respectively (Fig. S4) when B_{iso} values varied in the range 1–2 Å^2. This uncertainty originated from the lack of information at high diffraction angle, likely produced by an inherent disorder of channel sites which also exhibited the geometrical irregularity expected from literature [19,26,53]: O_{ch} particularly represented a strongly distorted octahedron, with two short and two long *M*-O distances of ~1.9 Å and ~2.8 Å respectively. Bond valence sums (BVS) for the two differently coordinated sites (Tabs. S17–S20) mirrored this disorder, with values ranging between 1.312(1) and 1.825(1). Nevertheless, we detected an increasing preference of the M^{2+} cations for the T_{ch} site along the sequence FeQss – NiQss – CoQss– ZnQss; moreover, *M*-O distances at T_{ch} increasingly converged towards a single value (Tab. S21), exhibiting therefore higher regularity as in fully hexagonal Li-bearing Qss [26]. This tendency showed a linear correlation with the unit cell volume of the crystals (Fig. 6-a).

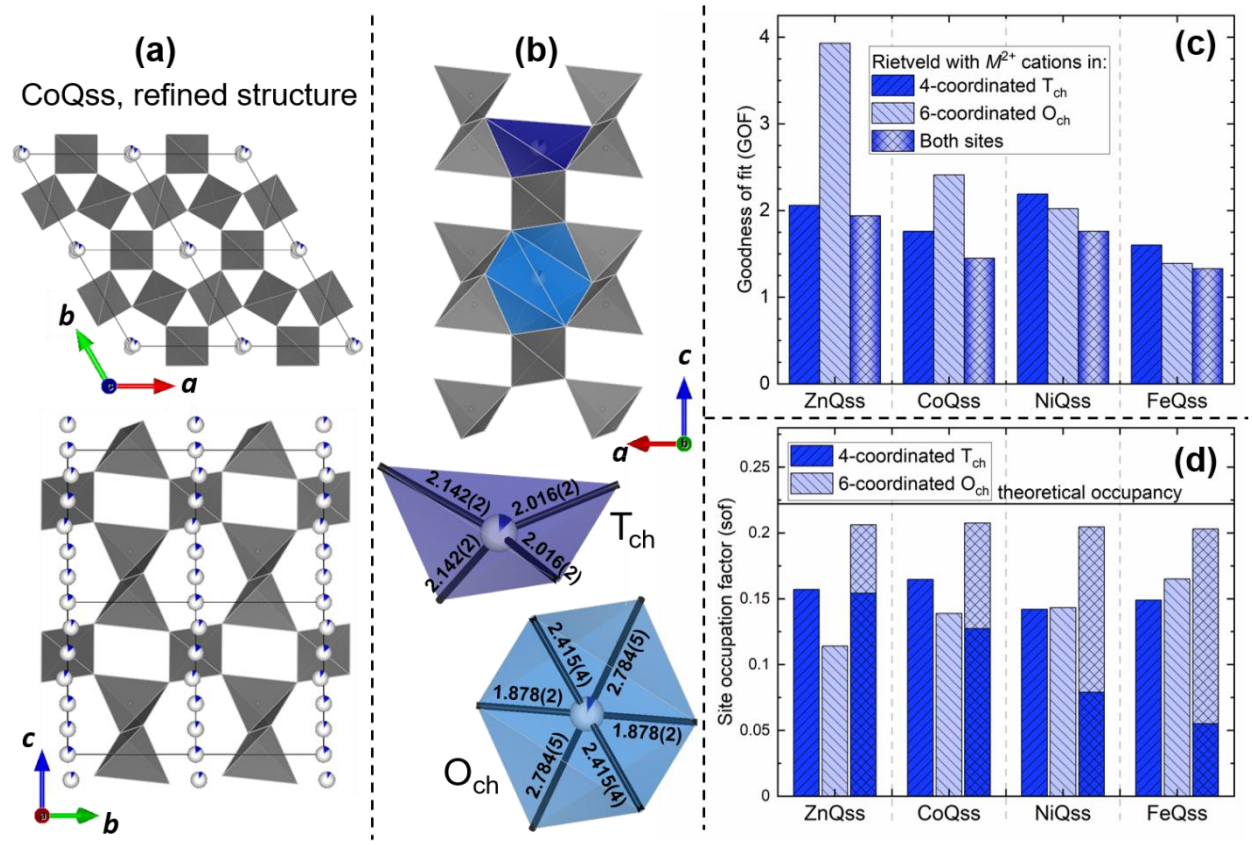

Figure 5. a) Best-fitting Qss structure obtained for the SPD data of sample CoQss, exhibiting a trigonal framework of tetrahedra (Al^{3+} and Si^{4+} statistically distributed) with Co^{2+} occupying both T_{ch} and O_{ch}, i.e. 4- and 6-coordinated channel sites (blue wedges represent the partial occupation at each site); b) details of the same structure, visualizing the 4- and 6-coordinated polyhedra occupied by Co^{2+} ions in the *c*-

channels with the respective Co-O bond distances in angstroms; c) goodness of fit (GOF) of Rietveld refinements performed on SPD data, with M^{2+} cations (M = Zn, Co, Ni or Fe) placed on T_{ch}, O_{ch} or both sites; d) site occupation factors (sof) obtained for M^{2+} cations from the same refinements (see related text for error evaluation).

Indeed, the sequence FeQss – NiQss – CoQss– ZnQss similarly defined an increase in structural pseudo-hexagonality, quantifiable through the AlO_4/SiO_4 tetrahedra tilt parameter δ formulated by previous authors [65] as:

$$\tan\delta = \frac{2\sqrt{3}}{9}\left(\frac{c}{a}\right)\frac{1-6z}{x}$$

where a, c, x and z are refinable lattice and atomic parameters in the quartz structure. For hexagonal high quartz δ = 0°, while trigonal low quartz yields δ = 16.3° (structural plots in Fig. S1). From the SPD refinements of our samples, we obtained 11.0(2)° for both NiQss and FeQss, 8.8(2)° for CoQss and 7.5(2)° for ZnQss; correlation with the unit cell volume of the crystals (Fig. 6-b) yielded a less clear trend than for sof values.

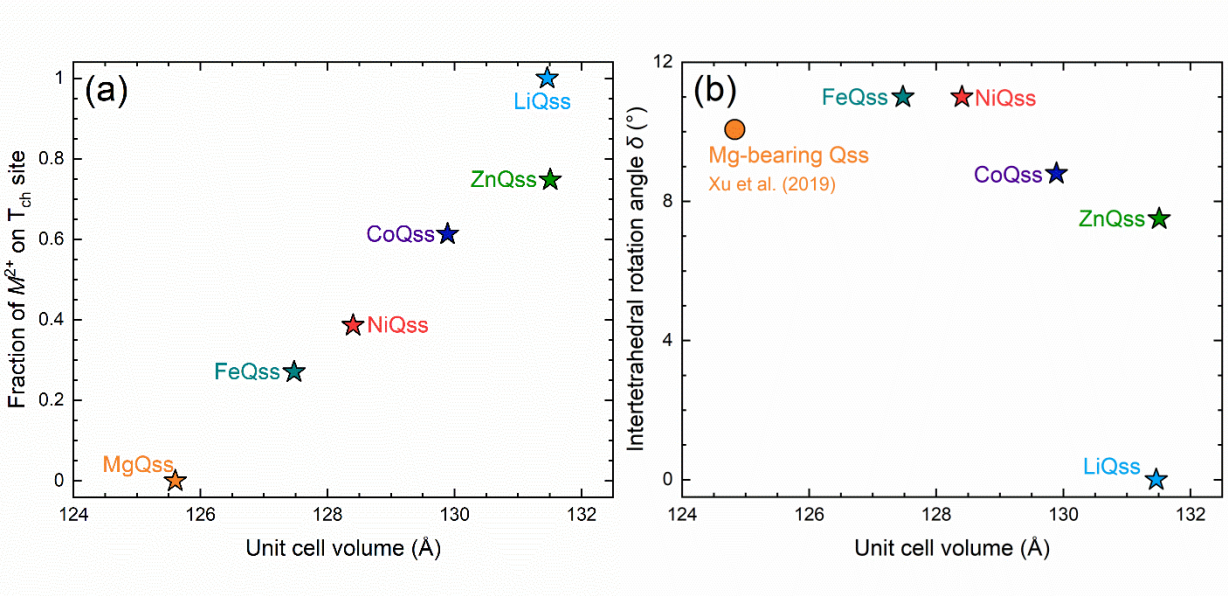

Figure 6. Correlations between values obtained from Rietveld refinements of SPD data: a) unit cell volume and fraction of the M^{2+} occupying the 4-coordinated channel site labelled as T_{ch} in Qss; b) unit cell volumes of Qss and respective pseudo-hexagonality angle δ. Data for Li- and Mg-bearing Qss (sof, δ angles) were retrieved or assumed from literature [19,53].

CoQss was additionally characterized by NPD to achieve better spatial resolution on the oxygen positions. Due to the higher amount of powder required for reasonable counting times during such measurement, a bigger batch (~4 g) was synthesized, obtaining in this case a phase-pure sample. We first performed a combined lab PXRD/NPD Rietveld refinement fixing all atomic thermal parameters to the

value of 1 $Å^2$ (Tab. S22), again due to the strong correlation between sof and thermal displacement parameters of Co^{2+}. Due to the very similar neutron scattering factors of Al^{3+} and Si^{4+} (3.449(5) fm and 4.149(1) fm, respectively), we were unable to reliably refine the Al/Si ratio in the tetrahedral framework sites, hence we constrained their occupations according to the refined Co^{2+} sof, to maintain charge balance in the structure. This approach yielded a good fit for lab PXRD, but intensity misfits were clearly observed for NPD data (R_{wp}= 3.99% GOF= 2.37); the obtained structural model agreed well with that extracted from SPD, yielding similar Co-O distances and pseudo-hexagonality (δ = 8.4(3)°). In the quest of improving the quality of neutron data fit, we additionally refined the B_{iso} parameter of the only non-equivalent oxygen atom, which increased to 2.93(7) $Å^2$. Such a high value suggests a strong positional disorder of Co^{2+} cations within the *c*-channels, inducing local displacements of the surrounding oxygen atoms. This structural model yielded a much better overall NPD data fit (Fig. S5 and Tab. S23) and lower reliability factors (R_{wp}= 3.50% GOF= 2.08) without repercussions on the PXRD fit; this structure resulted interestingly far more hexagonal (δ = 4(1)°), revealing the sensitivity of the δ parameter to the applied refinement strategy.

VT-PXRD measurements were performed between room temperature and 600 °C (lattice parameters in Tabs. S24 and S25) to study the thermal expansion behavior of the synthesized Qss (Fig. 7) and to compute their CTE in the range 30-300 °C (Tab. 1). All Qss exhibited a lower CTE than pure **SiO_2** quartz (12.5 x 10^{-6} K^{-1}) but distributed over a wide range of values: while the unit cell of ZnQss decidedly contracted upon heating (-2.2 x 10^{-6} K^{-1}), LiQss and CoQss closely approached zero thermal expansion (-0.7 x 10^{-6} K^{-1} and 0.2 x 10^{-6} K^{-1}, respectively). All other Qss expanded during the measurements, with $Co_{0.5}Ni_{0.5}$Qss exhibiting the lowest positive CTE among them (1.9 x 10^{-6} K^{-1}). In all cases, expansion along the *a*-direction was at least comparable or substantially higher than along the *c*-axis (Fig. S6): as manifested by the relative changes in c/a ratios (Fig. 7-b), LiQss showed the least isotropic behavior, whereas CoQss, NiQss and FeQss retained the initial values throughout the measurements.

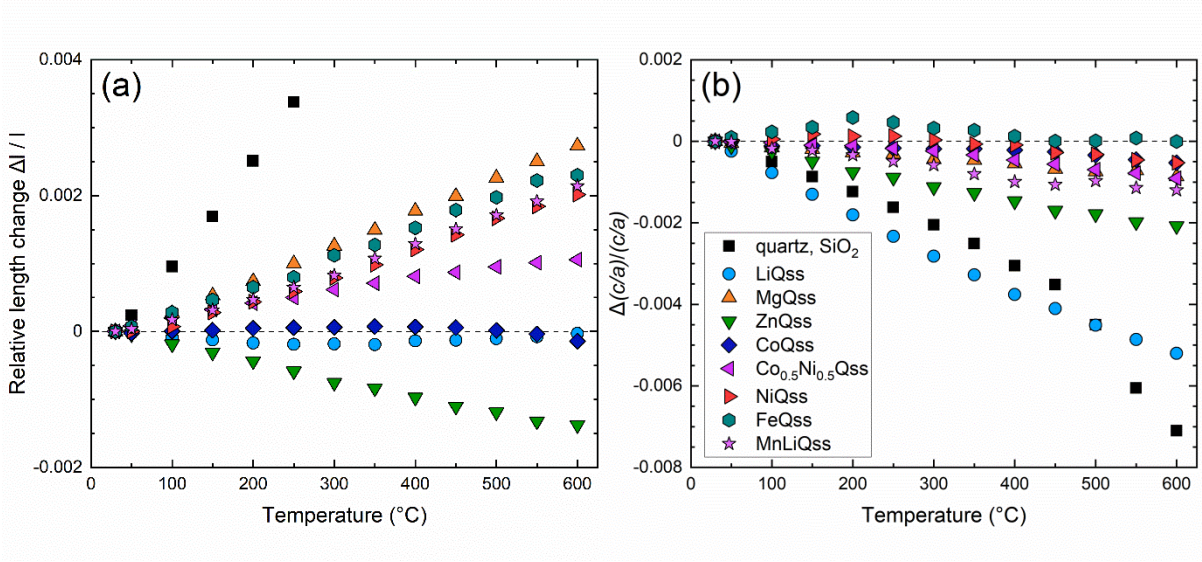

Figure 7. Results of VT-PXRD measurements performed **up to 600 °C to determine the thermal expansion of Qss phases contained in the studied samples**: a) relative average length change obtained from the unit cell volume of the crystals, referring to the radius of a sphere with the same volume; d) relative variation of the *c*/*a* ratio, providing the legend for both panels; error bars are smaller than the depicted symbols.

4. Discussion

Glass-ceramic powders containing Qss crystals stuffed with transition metal cations were synthesized for the first time within this work, relying on surface crystallization of glass powders and preferring short heat treatments to avoid the formation of more stable competing phases at these compositions, such as indialite/cordierite, spinel, non-stuffed quartz and cristobalite (see for instance Fig. S7 and previous literature [66–72]). Qss is commonly obtained as the first metastable devitrification product in a variety of aluminosilicate glasses containing Li, Mg and/or Zn [8,9], possibly due to close structural analogies with these amorphous precursors, in which Si^{4+} and Al^{3+} build up a network of interconnected tetrahedra with M^{+} and M^{2+} cations acting as charge compensators.

Aerodynamic levitation coupled to laser heating proved to be a very suitable method to synthesize the starting glasses, due to the minimization of heterogeneous nucleation in contactless conditions and the comparatively fast achievable cooling rates [44], of the order of 300 K s^{-1} (average rate over the first 1000 K). The choice of Ar as a levitation gas and the high melting temperatures (1800-2000 °C) were moreover crucial to retain transition metal ions predominantly in a reduced M^{2+} valence state, although EELS measurements could not unequivocally confirm the full stabilization of M^{2+} cations (particularly in sample MnLiQss). As known from literature, multivalent cations generally exhibit multiple coexisting oxidation states in glasses [73], which might have contributed to the difficult retrieval of high fractions of Qss in some of the samples (e.g. CoQss, FeQss and MnLiQss) and to the formation of some secondary phases

(e.g. metallic Ni in NiQss). Nonetheless, only FeQss required heat treatments in vacuum (an oxidizing atmosphere led to the formation of Fe_3O_4, Fe_2O_3 and mullite), while all other samples seemed less sensitive and could be crystallized in air. Even during high-temperature decomposition (Fig. S7), CoQss yielded non-stuffed quartz and $CoAl_2O_4$, hinting at a remarkable stability of the main initial oxidation state.

We achieved the best-fitting description of the average structure of Qss stuffed with transition metals using the less constrained trigonal model of low quartz, in agreement with recent results [18–21] that refuted the previously assumed [17,74] full hexagonality (i.e. the high-quartz-like character) of Mg-stuffed Qss. Furthermore, we allowed for Zn^{2+}, Co^{2+}, Ni^{2+} and Fe^{2+} to freely distribute over the two distinct channel positions reported for Li^+ and Mg^{2+} ions – respectively a distorted 4-coordinated site T_{ch} and a distorted 6-coordinated site O_{ch} (Fig. 5-b). Indeed, occupation of both tetrahedral and octahedral sites was previously reported in Zn-bearing Qss [27] and assigned spectroscopically to Ni^{2+} and Co^{2+} ions incorporated at impurity levels in Li-bearing Qss [39,40]. Mixed occupancy was identified in all Qss despite the inevitable uncertainties originating from the inherent disorder of channel sites, manifested by BVS calculations yielding lower values than 2 (Tabs. S4, S8, S12, S16) and by the high oxygen B_{iso} values obtained from the refined NPD data. Still, a preference for T_{ch} was invariably coupled to a bigger unit cell, even at constant Al/Si ratio in the tetrahedral sites (i.e. for all samples synthesized within this work, see Fig. 6), possibly hinting at higher size constraints for the occupation of these specific positions. The combined channel disorder, crystalline site distortion and defective local charge balancing (of which our best-fitting structural models clearly provide only an average description) may partially account for the pronounced metastability of Qss, as previously speculated by other authors [75].

The synthesis of Qss stuffed with Co^{2+} within this work specifically adds a new member to the restricted family of zero thermal expansion materials. The extremely low CTE (0.2×10^{-6} K^{-1}), negligible thermal expansion anisotropy (the c/a ratio changed only by 0.05% in the range 30-600 °C, compared to the 0.5% of LiQss) and simultaneously good stability against thermal decomposition (up to 900 °C at least, see Fig. S7) qualify this phase as a valid candidate for the future development of temperature-invariant or thermal-shock-resistant materials, potentially both in poly- and monocrystalline form. More generally, our results isolate the key structural factors determining the thermal expansion behavior of quartz-like phases, enhancing the fundamental understanding of these technologically relevant materials. As shown in Fig. 8, unit cell volumes exhibit a good linear correlation to the CTEs of quartz-like phases: this trend notably extends far beyond the results of this work, encompassing also several non-stuffed members of this family and without breaking down even in the transition from high- to low-quartz-like structures. On the contrary, a correlation between *c*/*a* ratios (mirroring cell distortions) and CTEs is only able to cluster the existing quartz-like phases into non-stuffed frameworks and stuffed Qss, adding little

information to what is obtainable from Fig. 3. Structural pseudo-hexagonality (i.e. the intertetrahedral tilt angle δ, Fig. S8) appears similarly inconclusive in rendering the thermal behavior of the crystals, although our coupled PXRD/NPD Rietveld refinements manifested a strong dependence of this latter parameter from the chosen refinement strategy, which could possibly affect the comparison between different literature sources.

Other authors [20,54] previously connected the thermal expansion of Qss ($LiAlSiO_4$ and $Mg_{0.5}AlSiO_4$) to three interdependent structural mechanisms: (i) a subtle deformation of Si/Al tetrahedra; (ii) positional disordering of channel cations with increasing temperature, so far identified only in superstructured Qss but possibly crucial in the crystals synthesized within this work, exhibiting simultaneous stuffing at T_{ch} and O_{ch} sites; (iii) tetrahedral tilting, which also represents the main process for the transformation from low to high quartz [65]. This latter mechanism appeared substantially hindered by channel stuffing (e.g. in $Mg_{0.5}AlSiO_4$ as compared to low quartz) [20], while it accounts for the slightly negative thermal expansion of hexagonal high quartz in the form of low-frequency, high-amplitude rigid unit modes [76]. It is therefore not surprising that highly Co-stuffed Qss exhibit the closest-to-zero CTE among all known Qss, given their almost full hexagonality at room temperature (i.e. an only limited range for tetrahedral tilting) and the most random distribution of channel stuffing cations between T_{ch} and O_{ch}.

To sum up, thermal expansion appears to be minimized in this system by any chemical substitution that is able to enlarge the room-temperature quartz unit cell, either by increasing the volume of the available framework sites (e.g. introducing Al^{3+} for Si^{4+}) or by occupying the otherwise vacant channel sites, thereby leading to a gradual distortion towards the hexagonal symmetry. Chemical stuffing of Qss is therefore a particularly efficient compositional strategy to synthesize crystals with low or negative CTE since it combines both mechanisms, i.e. tetrahedral expansion and framework gaping. In this context, full hexagonal symmetry does not appear a required condition for the synthesis of zero or negative thermal expansion quartz-like crystals.

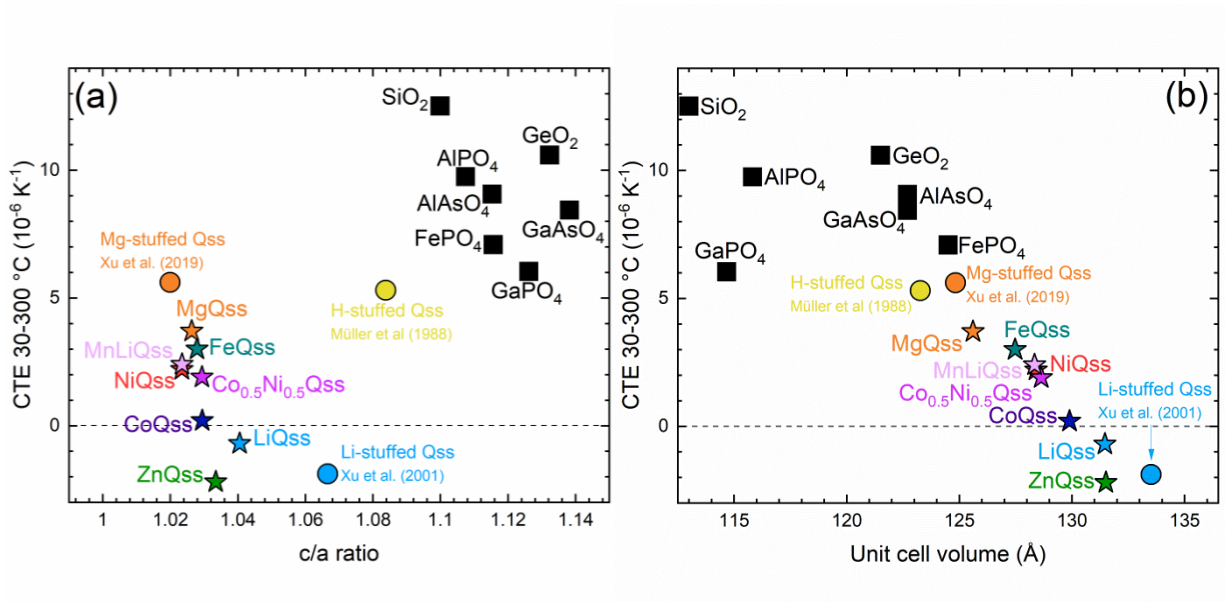

Figure 8. Correlations between: a) *c*/*a* lattice parameter ratio and CTE of quartz-like phases, with data from various literature sources [19,20,22,25,30,31,58,60,61,64,77]; c) unit cell volume and CTE of quartz-like phases, with data from various literature sources [20,22,31,60,65,77,78]. See also Fig. S8 of the supplementary materials. Error bars are smaller than the depicted symbols.

5. Conclusion

In addition to the well-known Li-, Mg- and/or Zn-stuffed quartz solid solutions, we report in this work the first synthesis of quartz-like aluminosilicate phases exclusively and heavily doped with transition metal cations (Fe^{2+}, Co^{2+}, Ni^{2+}, Mn^{2+}). The thermal expansion of these phases can be tuned finely and continuously from substantially negative (-2 x 10^{-6} K^{-1}) to strongly positive (~10 x 10^{-6} K^{-1}) values, relying on a smart compositional design within this enlarged chemical domain. Structural examination revealed that an overall expansion of the unit cell through framework substitutions and/or chemical stuffing is crucial for lowering the CTE of quartz-like phases, while framework distortion and pseudo-hexagonality appear less decisive. Most notably, the incredibly low thermal expansion coefficient (0.2 x 10^{-6} K^{-1} in the range 30 – 300 °C) of the newly synthesized Co-bearing quartz solid solutions is expected to stimulate the development of potentially Li-free zero-thermal-expansion (glass-)ceramics, reducing the technological dependence on critical raw materials such as lithium ores, whose market prices and availability have been impacted by the ever-growing battery industry.

Acknowledgement

Alessio Zandonà wishes to acknowledge the Deutsche Forschungsgemeinschaft (DFG) for funding his research through the Walter Benjamin Program, project n. 448961237, ZA 1188/1-1. Use of the Advanced Photon Source at Argonne National Laboratory was supported by the U. S. Department of

Energy, Office of Science, Office of Basic Energy Sciences, under Contract No. DE-AC02-06CH11357. This project has benefited from the facilities of the Platform MACLE-CVL co-funded by the European Union and Centre-Val de Loire Region (FEDER). The authors are grateful to Dr. Charles Hervoches and Dr. Premsyl Beran for performing the neutron diffraction measurement: it was carried out at the CANAM infrastructure of the Nuclear Physics Institute (Řež, Czech Republic) and infrastructure of reactors LVR-15 and LR-0, supported through the Ministry of Education, Youth and Sports project LM2015056 and LM2018120, respectively.

References

[1] W.L. Bragg, R.E. Gibbs, The structure of α and β quartz, Proc. R. Soc. Lond. A. 109 (1925) 405–427.

[2] H. Le Chatelier, Sur la dilatation du quartz, Bulletin de Minéralogie. 13 (1890) 112–118. https://doi.org/10.3406/bulmi.1890.2156.

[3] A. Ballato, Basic Material Quartz and Related Innovations, in: W. Heywang, K. Lubitz, W. Wersing (Eds.), Piezoelectricity: Evolution and Future of a Technology, Springer Berlin Heidelberg, Berlin, Heidelberg, 2008: pp. 9–35. https://doi.org/10.1007/978-3-540-68683-5_2.

[4] F.A. Hummel, Thermal Expansion Properties of Some Synthetic Lithia Minerals, Journal of the American Ceramic Society. 34 (1951) 235–239. https://doi.org/10.1111/j.1151-2916.1951.tb11646.x.

[5] M.J. Buerger, The stuffed derivatives of the silica structures, American Mineralogist. 39 (1954) 600–614.

[6] H.G.F. Winkler, Synthese und Kristallstruktur des Eukryptits, LiAlSiO4, Acta Crystallographica. 1 (1948) 27–34. https://doi.org/10.1107/S0365110X48000065.

[7] S.D. Stookey, Catalyzed Crystallization of Glass in Theory and Practice, Ind. Eng. Chem. 51 (1959) 805–808. https://doi.org/10.1021/ie50595a022.

[8] J. Petzoldt, Metastabile Mischkristalle mit Quarzstruktur mit Oxidsystem Li2O-MgO-ZnO-Al2O3-SiO2, Glastechnische Berichte. 40 (1967) 385–395.

[9] G.H. Beall, B.R. Karstetter, H.L. Rittler, Crystallization and Chemical Strengthening of Stuffed β-Quartz Glass-Ceramics, Journal of the American Ceramic Society. 50 (1967) 181–190. https://doi.org/10.1111/j.1151-2916.1967.tb15077.x.

[10] J. Deubener, M. Allix, M.J. Davis, A. Duran, T. Höche, T. Honma, T. Komatsu, S. Krüger, I. Mitra, R. Müller, S. Nakane, M.J. Pascual, J.W.P. Schmelzer, E.D. Zanotto, S. Zhou, Updated definition of glass-ceramics, Journal of Non-Crystalline Solids. 501 (2018) 3–10. https://doi.org/10.1016/j.jnoncrysol.2018.01.033.

[11] D. Krause, H. Bach, eds., Low Thermal expansion Glass Ceramics, Springer Berlin Heidelberg, 2005.

[12] G.H. Beall, Design and Properties of Glass-Ceramics, Annu. Rev. Mater. Sci. 22 (1992) 91–119. https://doi.org/10.1146/annurev.ms.22.080192.000515.

[13] P. Hartmann, R. Jedamzik, A. Carré, J. Krieg, T. Westerhoff, Glass ceramic ZERODUR®: Even closer to zero thermal expansion: a review, part 1, Journal of Astronomical Telescopes, Instruments, and Systems. 7 (2021) 1–23. https://doi.org/10.1117/1.JATIS.7.2.020901.

[14] P. Hartmann, R. Jedamzik, A. Carré, J. Krieg, T. Westerhoff, Glass ceramic ZERODUR®: Even closer to zero thermal expansion: a review, part 2, Journal of Astronomical Telescopes, Instruments, and Systems. 7 (2021) 1–27. https://doi.org/10.1117/1.JATIS.7.2.020902.

[15] S. Ray, Study of Ordering in High-Quartz Solid Solutions by Substitutions Affecting Superlattice Reflections, Journal of the American Ceramic Society. 56 (1973) 42–45. https://doi.org/10.1111/j.1151-2916.1973.tb12348.x.

[16] S. Ray, G.M. Muchow, High-Quartz Solid Solution Phases from Thermally Crystallized Glasses of Compositions (Li2O,MgO).Al2O3.nSiO2, Journal of the American Ceramic Society. 51 (1968) 678–682. https://doi.org/10.1111/j.1151-2916.1968.tb15927.x.

[17] W. Schreyer, J.F. Schairer, Metastable solid solutions with quartz-type structures on the join SiO2–MgAl2O4, Zeitschrift Für Kristallographie - Crystalline Materials. 116 (1961) 60–82. https://doi.org/10.1524/zkri.1961.116.1-2.60.

[18] M. Sternitzke, G. Müller, Crystal structure and thermal expansion of quartz-type aluminosilicates, Journal of Materials Science. 26 (1991) 3051–3056. https://doi.org/10.1007/BF01124841.

[19] H. Xu, P.J. Heaney, P. Yu, H. Xu, Synthesis and structure of a stuffed derivative of α-quartz, Mg0.5AlSiO4, American Mineralogist. 100 (2015) 2191–2198. https://doi.org/10.2138/am-2015-5303.

[20] H. Xu, X. Lü, P.J. Heaney, Y. Ren, Structural behavior of a stuffed derivative of α-quartz, Mg0.5AlSiO4, at high temperature: an in situ synchrotron XRD study, Physics and Chemistry of Minerals. 46 (2019) 717–725. https://doi.org/10.1007/s00269-019-01033-1.
[21] A. Zandona, B. Rüdinger, J. Deubener, Mg-bearing quartz solid solutions as structural intermediates between low and high quartz, Journal of the American Ceramic Society. 104 (2021) 1146–1155. https://doi.org/10.1111/jace.17517.
[22] H. Xu, P.J. Heaney, A. Navrotsky, Thermal expansion and structural transformations of stuffed derivatives of quartz along the LiAlSiO4–SiO2 join: a variable-temperature powder synchrotron XRD study, Physics and Chemistry of Minerals. 28 (2001) 302–312. https://doi.org/10.1007/s002690100165.
[23] A. Zandona, G. Helsch, J. Deubener, Inversion of quartz solid solutions at cryogenic temperatures, Journal of the American Ceramic Society. 103 (2020) 6630–6638. https://doi.org/10.1111/jace.17393.
[24] A. Zandona, G. Helsch, A. Martínez Arias, A.P. Weber, J. Deubener, Spray-dried sol-gel glass-ceramic powders based on the tunable thermal expansion of quartz and keatite solid solutions, Journal of the American Ceramic Society. 105 (2022) 207–216. https://doi.org/10.1111/jace.18057.
[25] G. Müller, M. Hoffmann, R. Neeff, Hydrogen substitution in lithium-aluminosilicates, Journal of Materials Science. 23 (1988) 1779–1785. https://doi.org/10.1007/BF01115722.
[26] C.-T. Li, The crystal structure of LiAlSi2O6 III (high-quartz solid solution), Zeitschrift Für Kristallographie - Crystalline Materials. 127 (1968) 327–348. https://doi.org/doi:10.1524/zkri.1968.127.16.327.
[27] M. Behruzi, Th. Hahn, Struktur und thermische ausdehnung des ungeordneten β-Eukryptits, Fortschr. Mineral. 55 (1977) 12–13.
[28] E.C. Shafer, R. Roy, Studies of Silica-Structure Phases: I, GaPO4, GaAsO4, and GaSbO4, Journal of the American Ceramic Society. 39 (1956) 330–336. https://doi.org/10.1111/j.1151-2916.1956.tb15598.x.
[29] E.C. Shafer, M.W. Shafer, R. Rustum, Studies of Silica Structure Phases II: Data on FePO4, FeAsO4, MnPO4, BPO4, AlVO4 and others, Zeitschrift Für Kristallographie. 108 (1956) 263–275. https://doi.org/doi:10.1524/zkri.1956.108.3-4.263.
[30] D. Schwarzenbach, Verfeinerung der Struktur der Tiefquarz-Modifikation von AlPO4, Zeitschrift Für Kristallographie. 123 (1966) 161–185. https://doi.org/doi:10.1524/zkri.1966.123.3-4.161.
[31] K. Kosten, H. Arnold, Die III-V-Analoga des SiO2, Zeitschrift Für Kristallographie - Crystalline Materials. 152 (1980) 119–134. https://doi.org/doi:10.1524/zkri.1980.152.14.119.
[32] G.S. Smith, P.B. Isaacs, The crystal structure of quartz-like GeO2, Acta Crystallographica. 17 (1964) 842–846. https://doi.org/10.1107/S0365110X64002262.
[33] A.F. Wright, A.N. Fitch, A.C. Wright, The preparation and structure of the α- and β-quartz polymorphs of beryllium fluoride, Journal of Solid State Chemistry. 73 (1988) 298–304. https://doi.org/10.1016/0022-4596(88)90113-2.
[34] J. Haines, C. Chateau, J.-M. Leger, R. Marchand, The use of composition and high pressure to extend the range of α-quartz isotypes, Ann. Chim. Sci. Mat. 26 (2001) 209–216.
[35] J. Petzoldt, Der Einbau von P2O5 in mestabile Mischkristalle mit Quarzstruktur des Grundsystems Li2O-MgO-ZnO-Al2O3-SiO2, Glastechnische Berichte. 41 (1968) 181–189.
[36] E.R. Segnit, T. Gelb, Metastable Quartz-Type Structures Formed from Kaolinite by Solid State Reaction, American Mineralogist. 57 (1972) 1505–1514.
[37] N. Takeuchi, M. Wakamatsu, Y. Hoshiyama, T. Yao, Formation of Quartz Solid Solution on Firing Kaolinite-CuO Mixtures and Its Structure, Journal of the Ceramic Society of Japan. 97 (1989) 27–31. https://doi.org/10.2109/jcersj.97.27.
[38] N. Takeuchi, H. Takahashi, S. Ishida, F. Horiie, M. Wakamatsu, Mechanistic Study of Solid-State Reaction between Kaolinite and Ferrous Oxide at High Temperatures, Journal of the Ceramic Society of Japan. 108 (2000) 876–881. https://doi.org/10.2109/jcersj.108.1262_876.

[39] U. Kang, O.S. Dymshits, A.A. Zhilin, T.I. Chuvaeva, G.T. Petrovsky, Structural states of Co(II) in β-eucryptite-based glass-ceramics nucleated with ZrO2, Journal of Non-Crystalline Solids. 204 (1996) 151–157. https://doi.org/10.1016/S0022-3093(96)00411-5.
[40] O.S. Dymshits, A.A. Zhilin, T.I. Chuvaeva, M.P. Shepilov, Structural states of Ni(II) in glasses and glass-ceramic materials of the lithium-aluminium-silicate system, Journal of Non-Crystalline Solids. 127 (1991) 44–52. https://doi.org/10.1016/0022-3093(91)90399-Q.
[41] A. Zandonà, S. Ory, C. Genevois, E. Véron, A. Canizarès, M.J. Pitcher, M. Allix, Glass formation and devitrification behavior of alkali (Li, Na) aluminosilicate melts containing TiO2, Journal of Non-Crystalline Solids. 582 (2022) 121448. https://doi.org/10.1016/j.jnoncrysol.2022.121448.
[42] G. Müller, H. Paulus, J. Stiefel, Synthesis and structure of β-quartz type Na0.5H0.5AlSi2O6 as compared to LiAlSi2O6, Neues Jahrbuch Fur Mineralogie-Monatshefte. 11 (1990) 493–503.
[43] C. Xu, Q. Dai, L. Gaines, M. Hu, A. Tukker, B. Steubing, Future material demand for automotive lithium-based batteries, Communications Materials. 1 (2020) 99. https://doi.org/10.1038/s43246-020-00095-x.
[44] A. Zandonà, M. Moustrous, C. Genevois, E. Véron, A. Canizarès, M. Allix, Glass-forming ability and ZrO2 saturation limits in the magnesium aluminosilicate system, Ceramics International. (2021). https://doi.org/10.1016/j.ceramint.2021.12.051.
[45] S. Degterov, A.D. Pelton, Critical evaluation and optimization of the thermodynamic properties and phase diagrams of the CrO-Cr2O3-SiO2 and CrO-Cr2O3-SiO2-Al2O3 systems, Journal of Phase Equilibria. 17 (1996) 488–494. https://doi.org/10.1007/BF02665995.
[46] P.P. Keat, A New Crystalline Silica, Science. 120 (1954) 328–330. https://doi.org/10.1126/science.120.3113.328.
[47] C.-T. Li, D.R. Peacor, The crystal structure of LiAlSi2O6-II ("β spodumene"), Zeitschrift Für Kristallographie. 126 (1968) 46–65. https://doi.org/doi:10.1524/zkri.1968.126.1-3.46.
[48] K. Kamiya, T. Yoko, K. Moroishi, K. Matusita, S. Sakka, Structural changes of glass-ceramics of the Cu2O-Al2O3-SiO2 system on heating in air, Journal of Materials Science. 21 (1986) 131–136. https://doi.org/10.1007/BF01144710.
[49] A.A. Coelho, TOPAS and TOPAS-Academic: an optimization program integrating computer algebra and crystallographic objects written in C++, Journal of Applied Crystallography. 51 (2018) 210–218. https://doi.org/10.1107/S1600576718000183.
[50] A. Zandona, B. Rüdinger, O. Hochrein, J. Deubener, Crystallization and SiAl ordering in cordierite glass-ceramics, Journal of Non-Crystalline Solids. 498 (2018) 160–166. https://doi.org/10.1016/j.jnoncrysol.2018.06.013.
[51] A. Zandona, B. Rüdinger, O. Hochrein, J. Deubener, Chemical gradients at the surface of TiO2-doped cordierite glass-ceramics, Journal of Non-Crystalline Solids. 547 (2020) 120298. https://doi.org/10.1016/j.jnoncrysol.2020.120298.
[52] J.-Y. Hsu, R.F. Speyer, Comparison of the Effects of Titania and Tantalum Oxide Nucleating Agents on the Crystallization of Li2O · Al2O3· 6SiO2 Glasses, Journal of the American Ceramic Society. 72 (1989) 2334–2341. https://doi.org/10.1111/j.1151-2916.1989.tb06085.x.
[53] H. Xu, P.J. Heaney, G.H. Beall, Phase transitions induced by solid solution in stuffed derivatives of quartz: A powder synchrotron XRD study of the LiAlSiO4-SiO2 join, American Mineralogist. 85 (2000) 971–979. https://doi.org/10.2138/am-2000-0711.
[54] H. Xu, P.J. Heaney, D.M. Yates, R.B. Von Dreele, M.A. Bourke, Structural mechanisms underlying near-zero thermal expansion in β-eucryptite: A combined synchrotron x-ray and neutron Rietveld analysis, Journal of Materials Research. 14 (1999) 3138–3151. https://doi.org/10.1557/JMR.1999.0421.
[55] D.P. Abraham, R.D. Twesten, M. Balasubramanian, J. Kropf, D. Fischer, J. McBreen, I. Petrov, K. Amine, Microscopy and Spectroscopy of Lithium Nickel Oxide-Based Particles Used in High Power Lithium-Ion Cells, Journal of The Electrochemical Society. 150 (2003) A1450–A1456.

[56] H. Tan, J. Verbeeck, A. Abakumov, G. Van Tendeloo, Oxidation state and chemical shift investigation in transition metal oxides by EELS, Ultramicroscopy. 116 (2012) 24–33. https://doi.org/10.1016/j.ultramic.2012.03.002.
[57] H.K. Schmid, W. Mader, Oxidation states of Mn and Fe in various compound oxide systems, Micron. 37 (2006) 426–432. https://doi.org/10.1016/j.micron.2005.12.004.
[58] M.A. Carpenter, E.K.H. Salje, A. Graeme-Barber, B. Wruck, M.T. Dove, K.S. Knight, Calibration of excess thermodynamic properties and elastic constant variations associated with the alpha <-- >beta phase transition in quartz, American Mineralogist. 83 (1998) 2–22. https://doi.org/10.2138/am-1998-1-201.
[59] F. Dachille, L.S. Dent Glasser, High pressure forms of BPO4 and BAsO4 quartz analogues, Acta Crystallographica. 12 (1959) 820–821. https://doi.org/10.1107/S0365110X59002365.
[60] E. Philippot, P. Armand, P. Yot, O. Cambon, A. Goiffon, G.J. McIntyre, P. Bordet, Neutron and X-Ray Structure Refinements between 15 and 1073 K of Piezoelectric Gallium Arsenate, GaAsO4: Temperature and Pressure Behavior Compared with Other α-Quartz Materials, Journal of Solid State Chemistry. 146 (1999) 114–123. https://doi.org/10.1006/jssc.1999.8316.
[61] A. Goiffon, J.-C. Jumas, M. Maurin, E. Philippot, Etude comparée à diverses températures (173, 293 et 373°K) des structures de type quartz α des phases MIIIXVO4 (MIII = Al, Ga et XV = P, As), Journal of Solid State Chemistry. 61 (1986) 384–396. https://doi.org/10.1016/0022-4596(86)90047-2.
[62] J.-M. Léger, J. Haines, L. Silva de Oliveira, C. Chateau, A. Le Sauze, R. Marchand, S. Hull, Crystal structure and high pressure behaviour of the quartz-type phase of phosphorous oxynitride PON, Journal of Physics and Chemistry of Solids. 60 (1999) 145–152.
[63] Roye et al., ICDD 00-032-1455, ICDD Grant-In-Aid. (1981).
[64] J. Haines, O. Cambon, E. Philippot, L. Chapon, S. Hull, A Neutron Diffraction Study of the Thermal Stability of the α-Quartz-Type Structure in Germanium Dioxide, Journal of Solid State Chemistry. 166 (2002) 434–441. https://doi.org/10.1006/jssc.2002.9625.
[65] H. Grimm, B. Dorner, On the mechanism of the α-β phase transformation of quartz, Journal of Physics and Chemistry of Solids. 36 (1975) 407–413. https://doi.org/10.1016/0022-3697(75)90066-9.
[66] U. Haefeker, R. Kaindl, P. Tropper, H. Krüger, V. Kahlenberg, M. Orlova, Structural investigations of the two polymorphs of synthetic Fe-cordierite and Raman spectroscopy of hexagonal Fe-cordierite, Mineralogy and Petrology. 108 (2014) 469–478. https://doi.org/10.1007/s00710-013-0313-3.
[67] K. Knorr, M. Meschke, B. Winkler, Structural and magnetic properties of Co2Al4Si5O18 and Mn2Al4Si5O18 cordierite, Physics and Chemistry of Minerals. 26 (1999) 521–529. https://doi.org/10.1007/s002690050215.
[68] F.J. Serrano, N. Montoya, J.L. Pizarro, M.M. Reventós, M.A. Kojdecki, J.M. Amigó, J. Alarcón, Crystal structure and microstructure of synthetic hexagonal magnesium–cobalt cordierite solid solutions (Mg2-2xCo2xAl4Si5O18), Acta Crystallographica Section B. 69 (2013) 110–121. https://doi.org/10.1107/S2052519213001401.
[69] T. Sugimura, H. Osato, Y. Nakai, The Metastable Zn-Indialite Crystallized out from the Glasses in the Ternary System ZnO-Al2O3-SiO2, Journal of the Ceramic Association, Japan. 82 (1974) 48–54. https://doi.org/10.2109/jcersj1950.82.48.
[70] M. Terada, K. Kawamura, I. Kagomiya, K. Kakimoto, H. Ohsato, Effect of Ni substitution on the microwave dielectric properties of cordierite, Journal of the European Ceramic Society. 27 (2007) 3045–3048. https://doi.org/10.1016/j.jeurceramsoc.2006.11.050.
[71] P. Wandschneider, F. Seifert, The System Magnesium Cordierite-Cobalt Cordierite, Journal of the American Ceramic Society. 67 (1984) C- 163-C- 164. https://doi.org/10.1111/j.1151-2916.1984.tb19182.x.

[72] F. Jose Torres, J. Alarcón, Phase evolution by thermal treatment of equimolar cobalt–magnesium cordierite glass powders, Journal of the European Ceramic Society. 24 (2004) 681–691. https://doi.org/10.1016/S0955-2219(03)00265-6.
[73] W.D. Johnston, Oxidation-Reduction Equilibria in Molten Na2O.2SiO2 Glass, Journal of the American Ceramic Society. 48 (1965) 184–190. https://doi.org/10.1111/j.1151-2916.1965.tb14709.x.
[74] H. Schulz, W. Hoffmann, G.M. Muchow, The average structure of Mg[Al2Si3O10], a stuffed derivative of the high-quartz structure, Zeitschrift Für Kristallographie - Crystalline Materials. 134 (1971) 1–27. https://doi.org/doi:10.1524/zkri.1971.134.16.1.
[75] C.-T. Li, Transformation mechanism between high-quartz and keatite phases of LiAlSi2O6 compositon, Acta Crystallographica Section B. 27 (1971) 1132–1140. https://doi.org/10.1107/S0567740871003649.
[76] M.G. Tucker, D.A. Keen, M.T. Dove, A detailed structural characterization of quartz on heating through the α–β phase transition, Mineralogical Magazine. 65 (2001) 489–507. https://doi.org/10.1180/002646101750377524.
[77] Y. Muraoka, K. Kihara, The temperature dependence of the crystal structure of berlinite, a quartz-type form of AlPO4, Physics and Chemistry of Minerals. 24 (1997) 243–253. https://doi.org/10.1007/s002690050036.
[78] E. Philippot, D. Palmier, M. Pintard, A. Goiffon, A General Survey of Quartz and Quartz-like Materials: Packing Distortions, Temperature, and Pressure Effects, Journal of Solid State Chemistry. 123 (1996) 1–13. https://doi.org/10.1006/jssc.1996.0145.